Channeling and optical study of thin Si crystals distorted by pressure

R. B. Alexander, P. J. Drallos, S. C. Johnson, and K. R. Padmanabhan
Department of Physics and Astronomy, Wayne State University, Detroit, Michigan 48202

J. C. Buchholz
Physics Department, General Motors Research Laboratories, Warren, Michigan 48090
(Received 28 December 1982)

The ion backscattering-channeling technique and reflection of laser light have been used to study the distortion of thin Si single crystals produced by a pressure differential across the crystal. For channeling in a Si-air cell, the channeled fraction at a fixed pressure decreases with increasing ion energy, beam diameter, and crystal area, and increases with crystal thickness. The threshold pressure for the abrupt decrease in the channeled fraction behaves in the same way. From an interference pattern observed in the reflected laser beam, the shape of the distorted Si surface can be deduced. The maximum deformation, which is a sublinear function of pressure, decreases with increasing crystal thickness. Calculations have been made of the channeled fraction from the results of the optical measurements, with the use of a geometric model in which the channeling minimum yield is determined by the distribution of angles of ion incidence over the bowed crystal surface. Comparison of calculated and measured values of the channeled fraction suggests that both rigidity and membrane stresses determine the crystal shape.

I. INTRODUCTION

Recently we reported[1] measurements of ion channeling in thin Si single crystals as a function of a pressure differential across the crystal. These measurements are part of a study of solid-liquid interfaces using ion backscattering and channeling. Energetic ions strike one side of a very thin single crystal (thickness $\sim 1\ \mu$m) in vacuum and interact with impurity atoms or displaced lattice atoms on the other side of the crystal at a solid-liquid interface. Channeled ions backscattered at the interface are detected in vacuum after traveling back through the crystal. Si crystals were chosen as these can be readily thinned by a standard technique which leaves a thin window supported by the bulk crystal. Because of the pressure differential between the vapor pressure of the liquid on one side of the window and vacuum on the other, the window bows out into the vacuum. The effect of this distortion on ion channeling is being investigated initially by experiments on solid-air interfaces, using Si-air cells in which the air pressure can be varied.

In our previous study it was found that the minimum yield $\chi_{\min}$ for axial channeling increases abruptly (from its value for an undistorted crystal) at a threshold pressure of several Torr, and approaches the random level at 50—100 Torr. The behavior of $\chi_{\min}$ with pressure was found to depend on the beam diameter and energy. In the present work the effect of the thickness and area of the Si window have been investigated, and further measurements have been made of the energy dependence. All these factors influence the pressure variation of $\chi_{\min}$, or of the channeled fraction $1-\chi_{\min}$.

Measurements were also made previously of the window deformation as a function of pressure using reflection of laser light, which produces an unusual interference pattern. Here we give details of the laser measurements and report results for the dependence of the deformation on thickness. To explain the channeling results we have proposed[1] a geometric model, in which $\chi_{\min}$ is determined by the tilting away from the beam direction of the channels perpendicular to the curved crystal surface, the shape of the surface being deduced from the laser interference pattern. In this paper the surface shape is discussed in more detail. Differences between values of $1-\chi_{\min}$ calculated from the optical data and the measured values are also discussed.

II. EXPERIMENTAL PROCEDURE

A. Sample preparation

Thin self-supporting Si single crystals can be prepared by a variety of techniques.[2] The technique used in this work involves[3] boron diffusion into a Si wafer followed by etching, first with a fast, nonselective etchant and then with slower ethylene diamine-pyrocatechol (EDP) etchant which does not attack heavily boron-doped Si. To define the window area we used one of two methods. In the first method the window is etched through a hole in a photoresist mask, which is hardened by proton bombardment (in an ion implanter) prior to etching. An alternative procedure involves initial fine-grit sandblasting through a hole in a metal mask. No differences were detected in windows prepared by the two methods.

All the wafers used were of (100) orientation. Regardless of the shape of the defining hole in the mask, a (100) window eventually acquires a rectangular shape with sides parallel to $\langle 110\rangle$ directions if the EDP etching time is long enough, due to the anisotropic etch rate and undercutting.[2] For this geometry the pit behind the window has side walls which are (111) surfaces. Our windows were typically 2.0—2.5 mm square, though in some cases where a round mask was used the window had cutaway corners (parallel to $\langle 100\rangle$ directions).

A Si-air cell is shown schematically in Fig. 1(b). The cell consists of a cavity, to which air (or another gas) can be admitted following evacuation, behind the self-supporting Si crystal.

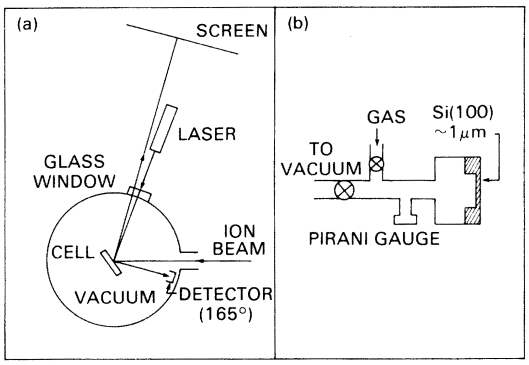

FIG. 1. Schematic diagrams of (a) the target chamber used for the channeling experiments and optical measurements, and (b) a Si-air cell assembly.

B. Channeling experiments

Channeling experiments were carried out with $^4He^+$ ions from the Wayne State University 4.75-MV Van de Graaff accelerator. The angular divergence of the incident beam was less than $\pm 0.02°$. The Si-air cell was mounted on a two-axis goniometer which has an accuracy and reproducibility of 0.01°; the goniometer could be translated in a direction parallel to the crystal surface. To measure the ion dose the target current was integrated, with suitable secondary electron suppression. Typical beam currents were 1—5 nA. Backscattered particles were detected with a 50-mm^2 Si surface barrier detector (energy resolution $\simeq$15 keV for ^{4}He), located at a scattering angle of 165° [Fig. 1(a)].

Air was admitted to the cell, or the cell evacuated, via a manifold attached to the target chamber. The cell pressure was measured with a Convectron gauge (manufactured by Granville-Phillips Company). The pressure outside the cell was maintained by turbomolecular pump at less than 1×10^{-7} Torr, and the vacuum inside the cell before each experiment commenced was less than 5×10^{-7} Torr.

C. Optical measurements

Optical measurements of the distortion were made by reflecting a parallel, or nearly parallel, laser beam from the curved surface of the Si window. A standard He-Ne laser ($\lambda=633$ nm) with a circular beam of diameter approximately 2 mm was used. The laser beam was incident on the Si-air cell at a small angle to the optical axis after passing through a glass port in the target chamber [Fig. 1(a)]. The reflected beam passed back through the glass port before being viewed on a screen placed approximately 2 m from the cell.

III. EXPERIMENTAL RESULTS

A. Channeling data

Backscattered energy spectra obtained for $^4He^+$ ions incident on a Si-air cell were presented in our earlier paper.[1] At high cell pressures the spectrum shows low-energy peaks due to scattering from nitrogen and oxygen in the air in the cell. Channeling measurements were made with the ion beam centered on the cell window, and the window aligned so that optimum channeling along the ⟨100⟩ axis was observed with vacuum in the cell. A random spectrum was taken in a direction near the ⟨100⟩ axis immediately after the initial alignment. The channeling is characterized by the minimum yield χ_{min}, which is defined as the ratio of the aligned to random yield just behind the Si front-surface peak and is the *non*channeled fraction of the beam at the front surface of the window. All the measurements reported here are for a beam diameter of 1 mm.

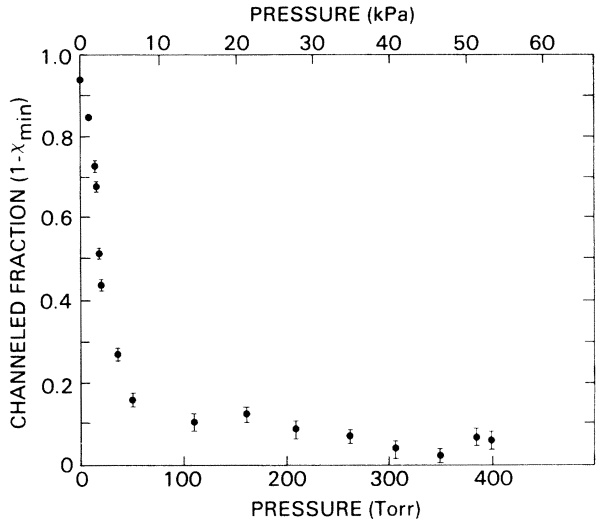

FIG. 2. ⟨100⟩ channeled fraction as a function of cell pressure for a 2.0-MeV $^4He^+$ beam incident on a Si(100)-air cell. The thickness of the cell window was 0.70 μm.

Figure 2 shows typical data obtained over the pressure range from less than 5×10^{-7} to 400 Torr. Our results in the present paper are expressed in terms of the channeled fraction of the beam, $1-\chi_{min}$, rather than χ_{min} as in our previous paper. Above the threshold pressure, which is not clearly discernible in Fig. 2, the channeled fraction is seen to decrease rapidly from an initial value of approxi-

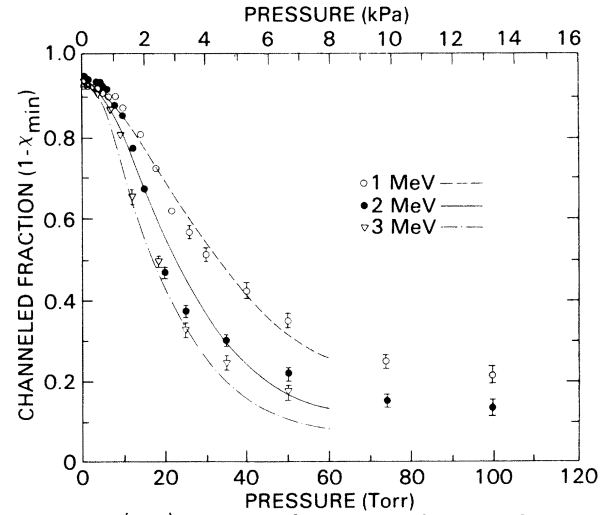

FIG. 3. ⟨100⟩ channeled fraction as a function of cell pressure for a $^4He^+$ beam of three different energies incident on a Si(100)-air cell. The cell window was 1.0 μm thick. The smooth curves are theoretical values of $1-\chi_{min}$ calculated from the optical measurements (Fig. 8) using the geometric model described in Sec. IV C.

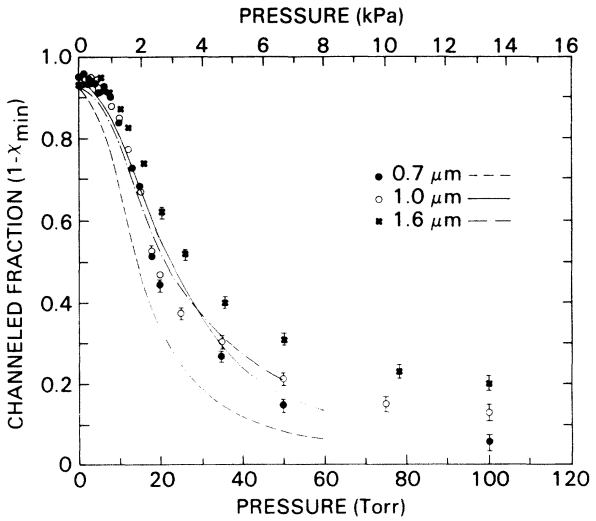

FIG. 4. ⟨100⟩ channeled fraction as a function of cell pressure for a 2.0-MeV $^4He^+$ beam incident on a Si(100)-air cell with windows of three different thicknesses. The window areas were approximately the same, being 2.2×2.2, 2.6×2.6, and 2.5×2.5 mm^2 for the 0.70-, 1.0-, and 1.6-μm-thick windows, respectively. The smooth curves are theoretical values of $1-\chi_{min}$ calculated from the optical measurements (Fig. 8) using the geometric model described in Sec. IV C.

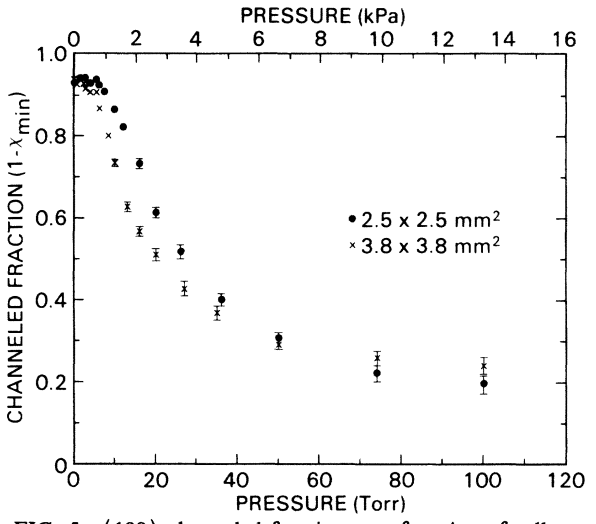

FIG. 5. ⟨100⟩ channeled fraction as a function of cell pressure for a 2.0-MeV $^4He^+$ beam incident on a Si(100)-air cell with windows of two different areas. The thickness of the 2.5×2.5 mm^2 window was 1.6 μm; the thickness of the 3.8×3.8 mm^2 window, 1.9 μm.

mately 0.95 to a high-pressure limit close to zero, corresponding to an increase in χ_{min} from approximately 0.05 to nearly 1.0. If the pressure was increased beyond 300–400 Torr, the window usually ruptured.

In Fig. 3 the variation of $1-\chi_{min}$ with pressure up to 100 Torr is shown for three different ion energies. The same Si window was used in each case. It can be seen that with increasing energy, the threshold pressure (for the abrupt decrease in the channeled fraction) decreases, and at pressures above the threshold the channeled fraction becomes smaller. A larger change occurs from 1 to 2 MeV than from 2 to 3 MeV.

The dependence on window thickness of the pressure variation of $1-\chi_{min}$ is illustrated in Fig. 4. This shows results for a $^4He^+$ beam of fixed energy (2.0 MeV) incident on three windows of different thickness and of approximately the same area. The thickness was determined from the backscattered energy spectrum. Comparison of Figs. 3 and 4 shows that the effect of increasing the window thickness is qualitatively similar to decreasing the ion beam energy, the threshold pressure increasing slightly with thickness. Although the values of $1-\chi_{min}$ for the 0.70- and 1.0-μm-thick windows are almost the same, the difference due to the change in thickness is obscured here by the difference in the areas of these two windows (2.2×2.2 mm^2 and 2.6×2.6 mm^2, respectively).

The effect of the window area on the pressure variation of $1-\chi_{min}$ is demonstrated in Fig. 5. Unfortunately, it was not possible to prepare two windows of different area but of the same thickness; the smaller area window was 1.6 μm thick, the larger area window 1.9 μm thick. However, the results show clearly that increasing the area of the window lowers the threshold pressure. It is evident from the thickness-dependence measurements (Fig. 4) that the area effect in Fig. 5 would be even larger if the two windows were of the same thickness. At the highest pressures investigated (50–100 Torr), there appears to be little dependence of $1-\chi_{min}$ on area.

B. Optical data

When the size of the laser beam was comparable to that of the Si window, a striking interference pattern was observed in reflection at almost all cell pressures. Typical patterns are presented in Fig. 6. The faint bands running across the dominant interference pattern (at ~30° to the vertical in Fig. 6) are due to interference effects in the glass port [Fig. 1(a)], while the oval-shaped feature in Fig. 6(b) is due to diffraction from dust on the glass. Reducing the size of the laser beam in general produced a pattern that was a part of the larger pattern, though for very small beams the interference pattern disappeared altogether. It was found that the four sharp cusps in the pattern correspond to the midpoints of the sides of the Si window, not the corners. The origin of the interference pattern will be discussed in Sec. IV. It is clear, however, that the size of the pattern, which is just the size of the reflected laser beam, is a measure of the angular spread of the reflected beam and thus of the window deformation.

In Fig. 7, the size of the pattern is plotted against pressure for a 0.70-μm-thick window. The size was arbitrarily taken to be the average value of the distance from the center of the pattern to a point midway between a corner and the midpoint of one of the sides of the pattern. Figure 7 also shows the number of interference fringes as a function of pressure. Good agreement is seen between the pressure dependence of the number of fringes and the pattern size (though the approximate correspondence of 100 fringes to a size of 200 mm is fortuitous). This result indicates that the number of fringes is also a direct measure of the distortion. It is possible that the actual number of fringes is slightly larger than the measured value, because of the difficulty in counting the number of fringes in the central bright spot. At pressures below 4 Torr, the pattern

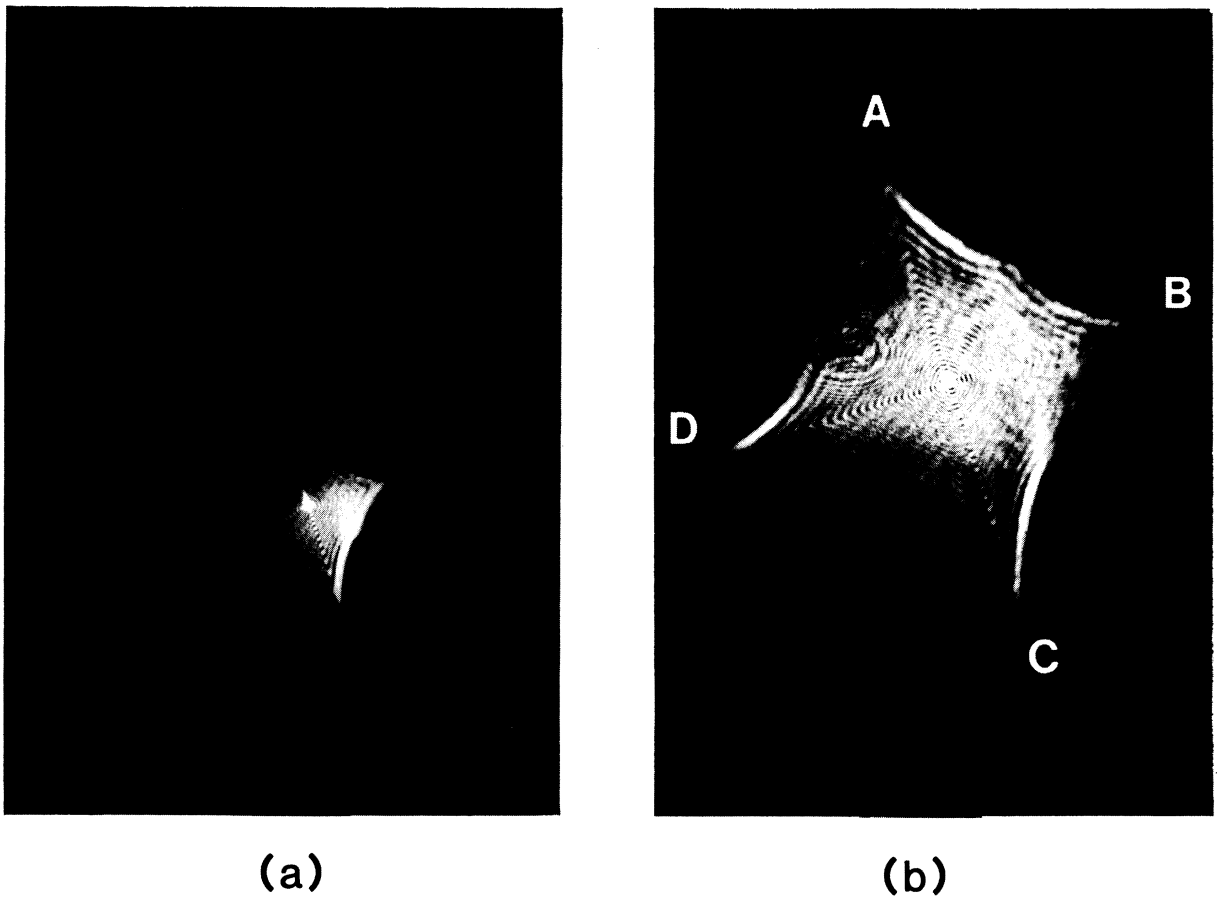

FIG. 6. Interference patterns observed in reflection of laser light ($\lambda = 633$ nm) from the window of a Si(100)-air cell, at cell pressures of (a) 5 Torr and (b) 11 Torr. The magnification is slightly different in each case. The small feature at the top left of (a) is due to reflection from the glass port of the target chamber.

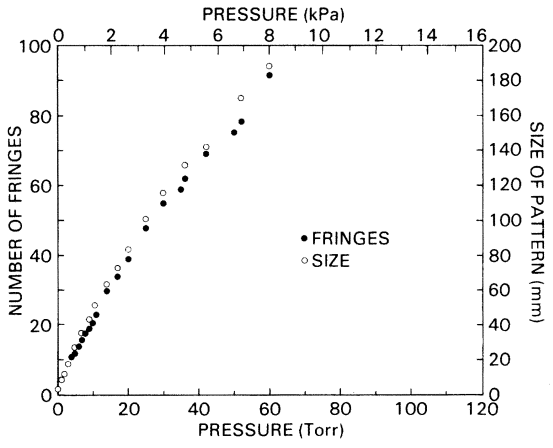

FIG. 7. Number of interference fringes and size of interference pattern as a function of cell pressure for a Si(100)-air cell with a window 0.70 μm thick. The pattern size is defined in the text (Sec. III B).

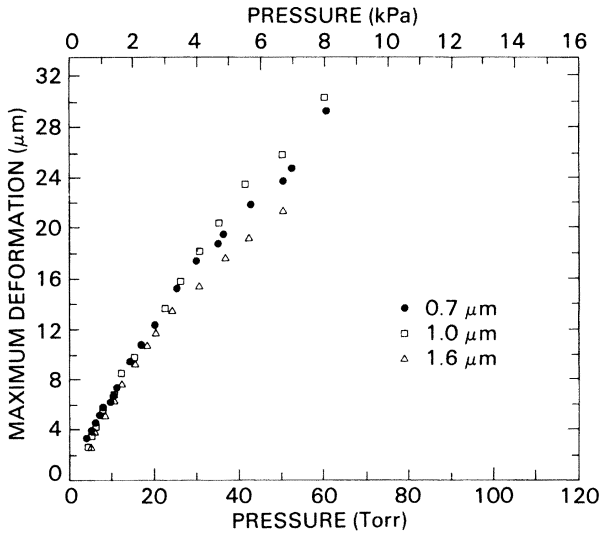

FIG. 8. Maximum deformation as a function of cell pressure for a Si(100)-air cell with windows of three different thicknesses. The deformation is calculated from the number of interference fringes, using Eq. (3).

was too small for the fringes to be counted accurately, while at pressures above 60 Torr all the fringes could not be counted because the pattern was obstructed by the glass port. Although the deformation, as measured by the number of fringes or the pattern size, increases smoothly with pressure, the dependence on pressure is seen from Fig. 7 to be sublinear.

Figure 8 shows the variation with pressure of the maximum deformation (at the center of the window) for three different window thicknesses. The deformation was determined from the number of interference fringes (see Sec. IV B). These measurements were made on the same three windows for which the channeling results in Fig. 4 were obtained. As in the case of the channeling measurements, the results for the 0.70- and 1.0-μm-thick windows cannot be compared directly because of the small difference in the areas of the two windows. Nevertheless, the difference between the results for the 1.0- and 1.6-μm-thick windows, which were of almost exactly the same area, shows that the maximum deformation depends inversely on the thickness. Optical measurements were not made on the large-area (3.8×3.8 mm^2) window.

IV. INTERPRETATION AND DISCUSSION OF RESULTS

A. Shape of surface

Information about the shape of the distorted Si window is contained in the laser interference pattern (Fig. 6), which is related to the Fourier transform of the wave field at the reflecting surface. The pattern can be characterized by its overall shape, the fringe spacing, and the number of fringes.

In optical language the boundary of the pattern is a caustic, of the type discussed by Berry,[4,5] the shape of the caustic being associated with the local curvature of the reflecting surface. The caustic (or outermost fringe) corresponds to reflection at the maximum angle, that is, from points of maximum slope in the plane of incidence or from a line of inflection on the surface. The curvature of the Si window is therefore not uniform. In the far-field region, the caustic is locally perpendicular to the associated line of inflection.[5] Figure 9 shows a curve which is constructed to be perpendicular to the caustic *ABCD* in Fig. 6(b), and which represents a projection of the line of inflection perpendicular to the direction of incidence. Although for the geometry here the pattern was observed in an intermediate region between the near field and far field, the curve should be at least a good qualitative indication of the inflection of the window surface (at the particular cell pressure). Inspection of Fig. 9 reveals that the projected line of inflection is closer to the center of the window along a window diagonal than along one of the lines *AC* or *BD* between the midpoints of opposite sides. This is in contrast to the probable height contours of the distorted surface which, for a square window, would be expected to be distended toward the corners. The window corresponding to Fig. 6 had cutaway corners (Sec. II A), but the diagonal was still the longest dimension. Thus the inflection line is not a line of constant height.

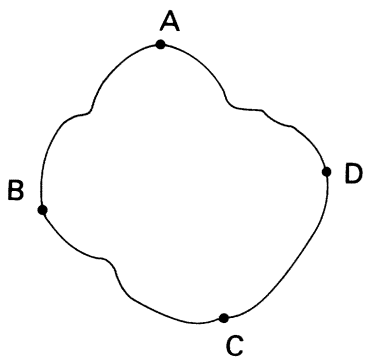

FIG. 9. Curve constructed to be locally perpendicular to the caustic labeled *ABCD* in Fig. 6(b). Note that this curve and the caustic are traversed in opposite senses.

In addition to the existence of a caustic, which implies nonuniform curvature, the cusps in the caustic provide further information about the surface topology. It can be seen in Fig. 6(b) that there are four sharp cusps, *A*, *B*, *C*, and *D* (corresponding to the midpoints of the sides of the window), as well as less pronounced, secondary cusps between the primary cusps. The cusps[5] correspond to local maxima and minima in the curvature of the line of inflection. These maxima and minima which are recognizable in Fig. 9 imply that the surface must have local "ridges," primarily in the directions from the center of the window to the midpoints of the sides, directions in which the greatest curvature in the plane of incidence (perpendicular to the undistorted surface) would be expected for a square window. Possibly the secondary cusps are due to secondary ridges along the diagonals, associated with the cutaway corners. The ridges may be associated partly with the crystalline properties of the Si, as well as with the shape of the window boundary.

Details of the surface shape could, in principle, be extracted from the interference pattern by making an appropriate optical transform. However, this would require detailed measurements of the fringe intensity. A simpler approach which we adopted is to assume that, to a first approximation, the surface is cylindrically symmetric. We then deduce the average surface shape from the measured fringe spacing using a two-beam interference model which we have proposed[6] to explain the interference pattern. In this model, a condition for the existence of fringes is a change of curvature (an inflection) of the window surface, the feature which also gives rise to a caustic. Thus when the size of the laser beam is less than the area enclosed by the line of inflection, the interference pattern disappears (Sec. III B). The requirement of an inflection rules out a spherical surface which has constant curvature, though such a surface would also have sharp edges which are physically unrealistic. We considered four possible surface shapes with smooth (built-in) edges. Of these, the one which gives the best agreement with the observed fringe spacing is a function

$$f(r)=f_0(1-r^2/a^2)^2 , \tag{1}$$

in which f_0 is the maximum deformation and a is the radius of the window. The other cylindrically symmetric shapes tried were a Gaussian function, a parabolic function, and a function of the form

$$f(r)=(f_0/2)[1+\cos(\pi r/a)] .$$

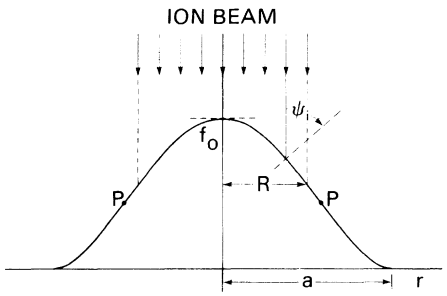

FIG. 10. Geometry for the calculations of the channeled fraction $1-\chi_{min}$. The solid curve is a cross section of the Si window surface, on an exaggerated scale, assuming the shape function of Eq. (1). The points P are points on the line of inflection which, for this shape, occurs at $r=0.58a$.

The function in Eq. (1) (see Fig. 10) is physically reasonable as it is the solution of the fourth-order differential equation for a clamped circular plate under uniform pressure, neglecting membrane (stretching) stresses[7]:

$$\frac{1}{r}\frac{d}{dr}\left\{r\frac{d}{dr}\left[\frac{1}{r}\frac{d}{dr}\left[r\frac{df}{dr}\right]\right]\right\}=\frac{P}{D}\ , \tag{2}$$

where P is the pressure and D is the flexural rigidity. It should be noted here that there is not an analytical solution to the differential equation for a clamped square plate under uniform pressure.

B. Maximum deformation

In our interference model[6] the fringes arise from interference between two rays reflected in the same direction from different parts of the surface. The outermost fringe corresponds to zero path difference between the two rays, the innermost fringe to a path difference equal to twice the maximum deformation f_0. Therefore, f_0 is proportional to the number N of bright or dark fringes, being given by

$$f_0=(N/2)\lambda\ , \tag{3}$$

where λ is the wavelength of the laser light.

As pointed out in Sec. III B, the maximum deformation is a sublinear function of pressure (Figs. 7 and 8). This contrasts with the linear dependence on pressure measured for distorted Si windows when the deformation is comparable to the window thickness,[8] unlike the large distortions in the present work.

C. Calculation of channeled fraction

Calculations have been made of the channeled fraction $1-\chi_{min}$ from the results of the optical measurements, in terms of a geometric model in which χ_{min} is determined by the distribution of incidence angles of the incoming ions relative to the channels perpendicular to the bowed window surface. Near the apex of the window the angle of incidence ψ_i is small and there will be little contribution to χ_{min}, but away from the apex ψ_i is larger (Fig. 10) and the contribution to χ_{min} may be appreciable. The distribution of angles depends on the shape of the surface, which in turn depends on the pressure. With the assumption of cylindrical symmetry, the channeled fraction can be expressed as

$$1-\chi_{min}=1-\frac{1}{\pi R^2}\int_0^{2\pi}\int_0^R \chi(\psi_i(r,f))r\,dr\,d\theta\ , \tag{4}$$

in which $\chi(\psi_i)$ describes the channeling angular yield for an undistorted window, f represents the shape of the distorted surface, and R is the radius of the ion beam.

The channeling dip $\chi(\psi_i)$ was also taken to be cylindrically symmetric, corresponding to an azimuthally averaged angular yield, and of the Gaussian form

$$\chi(\psi_i)=1-(1-\chi^0_{min})\exp[-0.693(\psi_i/\psi^0_{1/2})^2]\ , \tag{5}$$

with a minimum yield χ^0_{min} and half-angular width (critical angle) $\psi^0_{1/2}$ equal to those measured experimentally for a flat Si window. A Gaussian is a convenient analytical approximation to the shape of a channeling dip which has been used previously[9] under the conditions of an azimuthal average. For a surface of the shape given by Eq. (1) and for $\chi(\psi_i)$ given by Eq. (5), Eq. (4) becomes

$$1-\chi_{min}=(1-\chi^0_{min})(2/R^2)\int_0^R r\exp\{-[0.693/(\psi^0_{1/2})^2][\tan^{-1}(4f_0r^3/a^4-4f_0r/a^2)]^2\}dr\ . \tag{6}$$

Values of $1-\chi_{min}$ as a function of cell pressure were calculated by numerically integrating Eq. (6), with the maximum deformation f_0 given by Eq. (3), and the radius a taken as the average of the half-side and half-diagonal of the square window. Calculations based on the optical data for the 1.0-μm-thick window (Fig. 8) are included in Fig. 3, where smooth curves have been drawn through the individual points corresponding to the laser measurements. The three curves correspond to values of $1-\chi^0_{min}$ and $\psi^0_{1/2}$ at each of the three ion energies. Fairly good agreement is seen between the calculated and measured values of the channeled fraction, which decreases with increasing energy E because the channeling critical angle $\psi^0_{1/2}$ varies[10] as $E^{-1/2}$. As $\psi^0_{1/2}$ becomes smaller, a smaller fraction of the incident beam is channeled at a given pressure. The behavior of $1-\chi_{min}$ (or χ_{min}) with pressure and its dependence on energy are qualitatively similar to the variation observed in χ_{min} as a function of the spread of crystallite orientations in a polycrystalline layer.[9,11]

Calculations of $1-\chi_{min}$ based on the optical data of Fig. 8, for three different thicknesses, are included in Fig. 4. Although there is good qualitative agreement between calculated and measured values, the quantitative agreement is poorer than in Fig. 3. The apparent lack of correspondence between the calculated values in Fig. 4 and the laser measurements (Fig. 8) is associated with the small differences in the window areas, which affects $1-\chi_{min}$ through the radius a in Eq. (6). For the shape function in Eq. (1), f_0 is proportional to a^4/h^3 where h is the window thickness.[7] Thus the channeled fraction, which depends inversely on the deformation f_0, should increase with increasing window thickness and decrease with increasing area. This is consistent with the data presented in Figs. 4 and 5.

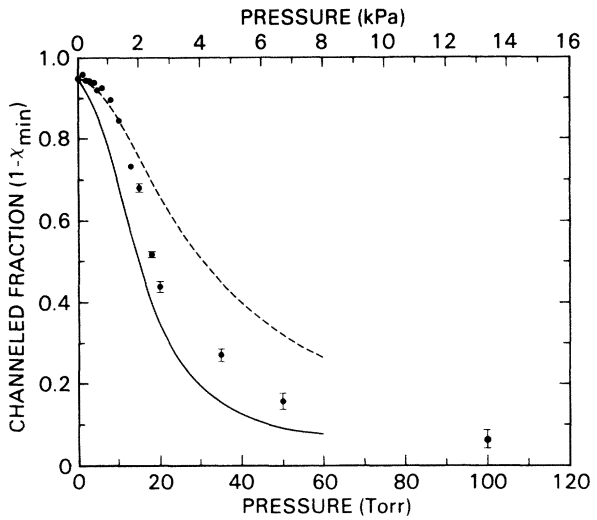

FIG. 11. Theoretical values of $1-\chi_{min}$ calculated from the optical measurements (Fig. 7), compared to the experimental values for a 0.70-μm-thick Si window. The solid curve is for a surface shape given by Eq. (1), the dashed curve for a spherical surface.

The lack of better quantitative agreement between calculated and measured values of $1-\chi_{min}$ is probably due in part to the assumption of a cylindrically symmetric surface. As discussed in Sec. IV A the actual surface shape is complex and includes local ridges. Although the calculated curves show a less abrupt change in $1-\chi_{min}$ than that measured experimentally, this is largely due to the Gaussian function [Eq. (5)] used to represent the channeling dip which here was determined to be more flat bottomed than a Gaussian. The approximately constant measured value of $1-\chi_{min}$ below the threshold pressure in Figs. 3–5 corresponds to angles of incidence within the flat-bottomed portion of the channeling dip.

It is likely that the addition of a membrane term to the shape function in Eq. (1) would improve the agreement between calculation and measurement. When membrane stresses are included in the one-dimensional differential equation [Eq. (2)], the solution cannot be completely determined but the maximum deformation f_0 is a sublinear function of the applied pressure,[7] as was observed in the optical measurements (Figs. 7 and 8). The solution of the differential equation including only membrane stresses and neglecting rigidity is a spherical surface. Calculations of $1-\chi_{min}$ for a spherical surface, even though physically unrealistic as pointed out previously, are compared to those for the surface shape of Eq. (1) in Fig. 11. It is seen that the spherical surface gives a good fit to the channeling data at low pressures, but at higher pressures the data points lie between the two curves. This suggests that the surface shape changes with pressure and, in the approximation of cylindrical symmetry, is somewhere between the shape given by Eq. (1) and a purely spherical surface.

V. CONCLUSIONS

The principal results of this study are the following: (i) For channeling in a Si-air cell, the channeled fraction $1-\chi_{min}$ at a fixed pressure *decreases* with increasing ion energy, beam diameter,[1] and window area, and *increases* with increasing window thickness. The threshold pressure for the abrupt decrease in $1-\chi_{min}$ (or increase in χ_{min}) behaves in the same way. In experiments on solid-liquid interfaces, where the largest possible channeled fraction at the back surface of the Si window is required, these four factors will need to be optimized. (ii) The maximum deformation of the Si window, determined from the interference pattern observed with reflected laser light, decreases with increasing window thickness. The deformation is a sublinear function of pressure. (iii) The shape of the distorted Si surface deduced from the interference pattern is complex and includes local ridges. In the approximation of cylindrical symmetry, the shape most consistent with the observed fringe spacing is a function of the form

$$f(r)=f_0(1-r^2/a^2)^2 .$$

(iv) The channeling results can be explained by a geometric model in which the channeled fraction (or the minimum yield) is determined by the distribution of angles of ion incidence over the bowed window surface. This model predicts values of $1-\chi_{min}$ in good qualitative agreement with the experimental results, although quantitative agreement is limited by the approximation of cylindrical symmetry. Comparison of measured values of $1-\chi_{min}$ with values calculated for different surface shapes suggests that both rigidity and membrane stresses determine the actual shape.

ACKNOWLEDGMENTS

We wish to thank D. M. Heffelfinger and S. A. Khan for their assistance in this work, K. D. Wise for supplying the boron-diffused Si wafers, and L. G. Dishman for photographing the interference patterns. Stimulating conversations with I.-C. Khoo and J. R. Sambles are appreciated. We are grateful to B. F. Buxton for drawing our attention to the work of M. V. Berry. The work was supported by a grant from the National Science Foundation. A grant from Research Corporation is also acknowledged.

[1]R. B. Alexander, S. C. Johnson, K. R. Padmanabhan, and J. C. Buchholz, Appl. Phys. Lett. 42, 804 (1983).
[2]K. E. Petersen, Proc. IEEE 70, 420 (1982).
[3]N. W. Cheung, Rev. Sci. Instrum. 51, 1212 (1980).
[4]M. V. Berry, J. Phys. A 8, 566 (1975).
[5]M. V. Berry, Adv. Phys. 25, 1 (1976).
[6]P. J. Drallos and R. B. Alexander, Appl. Opt. 22, 1613 (1983).
[7]S. Timoshenko and S. Woinowsky-Krieger, *Theory of Plates and Shells*, 2nd ed. (McGraw-Hill, New York, 1959).
[8]K. W. Lee and K. D. Wise, IEEE Trans. Electron Devices ED-29, 34 (1982).
[9]D. Sigurd, R. W. Bower, W. F. Van der Weg, and J. W. Mayer, Thin Solid Films 19, 319 (1973).
[10]J. Lindhard, K. Dan. Vidensk. Selsk. Mat.-Fys. Medd. 34 (1965).
[11]H. Ishiwara and S. Furukawa, J. Appl. Phys. 47, 1686 (1976).

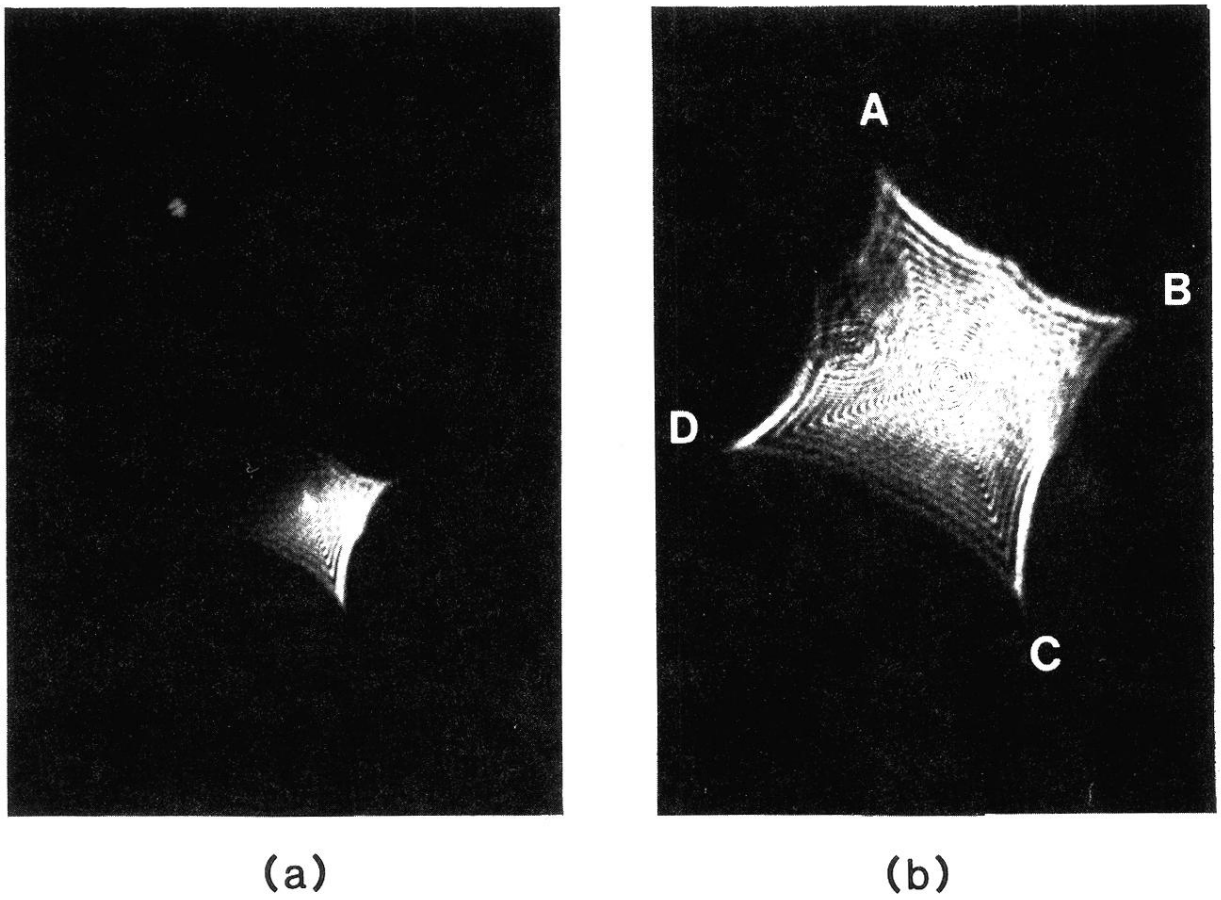

FIG. 6. Interference patterns observed in reflection of laser light ($\lambda = 633$ nm) from the window of a Si(100)-air cell, at cell pressures of (a) 5 Torr and (b) 11 Torr. The magnification is slightly different in each case. The small feature at the top left of (a) is due to reflection from the glass port of the target chamber.